Contents lists available at ScienceDirect

Fuel

journal homepage: www.elsevier.com

Full Length Article

Density functional theory study of CO formation through reactions of polycyclic aromatic hydrocarbons with atomic oxygen ($O(^3P)$)

Özlem Yönder*, Christof Hättig

Lehrstuhl für Theoretische Chemie, Ruhr-Universität Bochum, D-44780 Bochum, Germany

ARTICLE INFO

Keywords:
Polycyclic aromatic hydrocarbons
PAH
DFT
$O(^3P)$
CO formation
Oxy-fuel
Char
Combustion

ABSTRACT

To provide a qualitative analysis on how the reaction energies and mechanisms of initial steps of char combustion depend on a) the size of polycyclic aromatic hydrocarbons (PAHs) and b) the reaction sites, we investigate the initial steps of the individual reactions of thirteen PAHs with atomic oxygen with density functional theory. Specifically, we have studied three elementary steps: i) $O(^3P)$ addition, ii) subsequent oxyradical formation through H abstraction, and iii) CO elimination from the oxyradicals. We find that the CO elimination from the oxyradicals follows either a three, two, or single step mechanism, depending on the geometrical strain at the reaction site. In accordance, we observe that as the geometrical strain at the reaction site increases, the activation energy of the first step of the CO elimination from the oxyradicals increases. Important findings that are relevant for a multiscale modeling of the oxidation of large PAHs, e.g. during char burnout, are that the activation energies for these reactions can be related to the reaction energies through Bell-Evans-Polanyi (BEP) fits, and that for the O addition and the last step of the three or two step CO elimination mechanisms, i.e. the CO elimination from carbonyl radicals, the reaction energies are correlated with the stabilization energies calculated from the Hückel molecular orbital theory.

1. Introduction

The interest in oxy-fuel combustion in coal-fired power generation has been increasing during the last years due to its potential to reduce NO_x emissions and to capture CO_2 more easily as compared with conventional air combustion [1]. To optimize the combustion, an understanding of the reactions within an oxy-fuel atmosphere is crucial and, indeed, there is a body of studies focusing on the macroscopic and microscopic levels. However, atomistic studies of the reaction mechanisms are still rather uncommon.

Char includes amorphous and crystalline contents [2–4]. The amorphous content is composed of small, heat-resistant aliphatic and hetero(aromatic) elements such as phenols, quinones, pyrols, furans, and small polyaromatic units; whereas the crystalline part is composed of turbostratically stacked graphene layers [2]. Since both the amorphous and the crystalline content include aromatic structures, PAHs are important model systems to study the combustion of char. Additionally, the understanding of the oxidation of PAHs provides also important information on the oxidation of soot.

In the current contribution we studied initial steps of the reaction of atomic oxygen with PAHs of different sizes and at different reaction sites. Fig. 1 illustrates the different molecular regions of PAHs studied in this work. In IR spectroscopy of PAHs, the bending C–H vibrations of the molecular regions containing one (solo), two (duo), three (trio), or four (quartet) adjacent hydrogens show different frequency ranges [5]. The range is 900–860 cm^{-1} for the solo region, 860–800 cm^{-1} for the duo, 810–750 cm^{-1} for the trio and 770–735 cm^{-1} for the quartet regions [5]. The quartet and trio regions can further be differentiated by their relative location to the adjacent fused ring. The first carbon atom next to the neighboring ring is referred as inner (or α) and the second one as outer (or β) position. Another classification of positions as bay and fjord regions originates from NMR spectroscopy. The bay and fjord regions are sterically crowded; therefore, they show downfield shifts in NMR which are more pronounced for the fjord regions than the bay regions [5].

An important reaction which initiates the decomposition of polycyclic aromatic structures (C_xH_y) during combustion is the elimina-

* Corresponding author.
Email addresses: oezlem.yoender@theochem.ruhr-uni-bochum.de (Ö. Yönder); christof.haettig@theochem.ruhr-uni-bochum.de (C. Hättig)

https://doi.org/10.1016/j.fuel.2018.12.047
Received 2 May 2018; Received in revised form 4 October 2018; Accepted 5 December 2018
Available online xxx
0016-2361/ © 2018.

UNCORRECTED PROOF

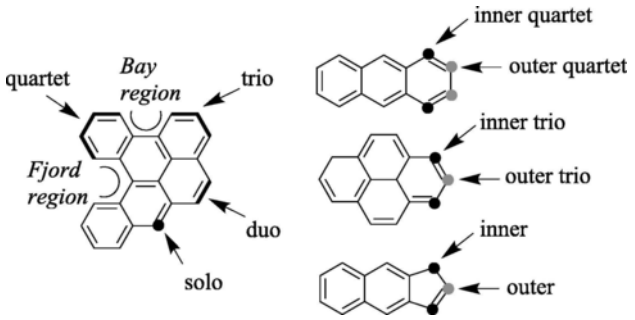


Fig. 1. Molecular regions of PAHs as classified in this work.

tion of CO from oxyradicals $C_xH_{y-1}O\cdot$. A pathway leading to the formation of oxyradicals can be the addition of an O_2 molecule to a PAH radical, followed by the cleavage of the O–O bond [6]:

$$C_xH_{y-1} + O_2 \rightarrow C_xH_{y-1}O_2 \rightarrow C_xH_{y-1}O + O(^3P). \quad (1)$$

A second oxyradical formation pathway is the addition of $O(^3P)$ to PAHs forming a diradical and the subsequent H abstraction,

$$C_xH_y + O \rightarrow C_xH_yO \rightarrow C_xH_{y-1}O + H, \quad (2$$

which can occur on the triplet potential energy surface. Following the formation of the oxyradical, CO can be eliminated as:

$$C_xH_{y-1}O \rightarrow C_{x-1}H_{y-1} + CO. \quad (3)$$

Atomic oxygen $O(^3P)$ can be formed in a high temperature environment together with other radicals such as H, OH, or HO_2 during the initiation process (the so-called radical pool formation) [7,8]. For example, Brezinsky suggested that phenyl radicals can be formed from benzene through abstraction of H [8]:

$$C_6H_6 \rightarrow C_6H_5 + H \quad (4)$$

For toluene proposed initiation processes are the thermal elimination of the low strength benzylic H:

$$C_6H_5CH_3 \rightarrow C_6H_5CH_2 + H, \quad (5)$$

or the abstraction of hydrogen by O_2 [8]:

$$C_6H_5CH_3 + O_2 \rightarrow C_6H_5CH_2 + HO_2. \quad (6)$$

The branching reaction of H with O_2 leads to the formation of the radicals OH and O [8]:

$$H + O_2 \rightarrow OH + O. \quad (7)$$

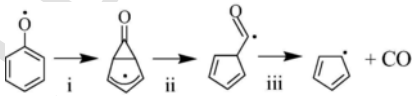
Another route for the formation of $O(^3P)$ is the above mentioned cleavage of the O-O bond in peroxy ($RO_2\cdot$) radicals.

Previous theoretical studies established that the most important pathway for the reaction of C_6H_6 with $O(^3P)$ starts with an electrophilic addition of $O(^3P)$ to benzene in the triplet state [9,10]. The calculated activation barrier of this reaction is 20.5 kJ/mol at the CBS-QB3 level [10] and 23.8 kJ/mol at the G3B3 level [9,10] of theory. Taatjes et al. observed, however, that in a flow reactor above 700 K, phenoxy $(C_6H_5O) + H$ and cyclopentadiene $(C_5H_6) + CO$ appear as products [9].

The diradical formed by the electrophilic addition of $O(^3P)$ to benzene can pass through an intersystem crossing by a nonradiative transition to the singlet state followed by the almost barrierless isomerization to benzene oxide with 230 kJ/mol energy release as calculated by CASSCF [9]. The singlet benzene oxide can rearrange to 2,4-cyclohexadienone with a barrier of 160 kJ/mol which can further isomerize to phenol or cyclopentadiene + CO with energy barriers of, respectively, 213 and 251 kJ/mol [9,10].

Nguyen et al. studied the formation of the cyclopentadienyl radical (C_5H_5) on the triplet surface from the diradical formed upon $O(^3P)$ addition to benzene through formyl cyclopentadiene (C_5H_5CHO) as intermediate [10]. Because of the high activation barrier of 135 kJ/mol (obtained from CBS-QB3) and lack of experimental evidence for C_5H_5 + CHO as products, they concluded that this route is not important for benzene [10].

Another reaction route that leads to the cyclopentadienyl radical is the decomposition of oxyradicals. An early theoretical study by Olivella et al. using CASPT2/6–31G-(d,p) and a later study by Lui et al. using CASSCF/6–31G* established that the elimination of CO from the phenoxy radical follows a three step mechanism: i) Formation of a bicyclic radical intermediate, followed by ii) a ring opening of its cyclopropanone moiety to a carbonyl radical, and finally, iii) CO elimination from the carbonyl yielding the cyclopentadienyl radical [11,12]:



(8)

Concerning larger PAHs, You et al. studied the decomposition of pentacene oxyradicals at the DFT B3LYP/6–311G(d,p) level [13]. On the outer quartet site the reaction follows a similar mechanism as for the phenoxy radical with activation barriers of 195, 42.3, and 10.5 kJ/mol for the three elementary reaction steps. On the inner quartet site, the barriers were found to be 238, 6.7, and 10.5 kJ/mol [13]. For the solo sites they could not find a similar reaction path [13]. Instead they found pathways with different intermediates which lead to ring openings with barriers around 440 kJ/mol [13]. Liu et al. did a similar study at the DFT B3LYP/6–311 + G(d,p) level for the decomposition of benz[a]anthracene oxyradicals at the outer quartet, bay-inner quartet, solo, and bay-solo positions and of H-cyclopenta[a]anthracene oxyradical as an example for the decomposition of a five-membered ring [14]. The energy barriers for the three steps were respectively 197, 74.9, and 10.8 kJ/mol for the outer quartet site, and 217, 16.3, and 14.2 kJ/mol for the bay-inner quartet site. In contrast to the studies on the pentacene oxyradicals, they were able to find at a solo site a reaction path similar to that of benzene but occuring in a single step instead of in three steps. The energy barrier for the single step elimination at the solo site was calculated as 348 kJ/mol and at the bay-solo site as 335 kJ/mol [14].

In the current contribution we report a study on the reactions of PAHs with $O(^3P)$ which lead to the formation of the oxyradicals

UNCORRECTED PROOF

(reaction (2)) and the subsequent elimination of CO (reaction (3)). Existing studies on these reactions covered only a few of the different possible site types mentioned above. As it is not feasible to treat all possible reaction sites for a sufficiently representative set of molecules (cmp. Fig. 2) with accurate wavefunction methods like CASPT2 and as we are aiming in the current study rather for the identification and understanding of trends transferable to larger PAHs we employ for the current study density functional theory.

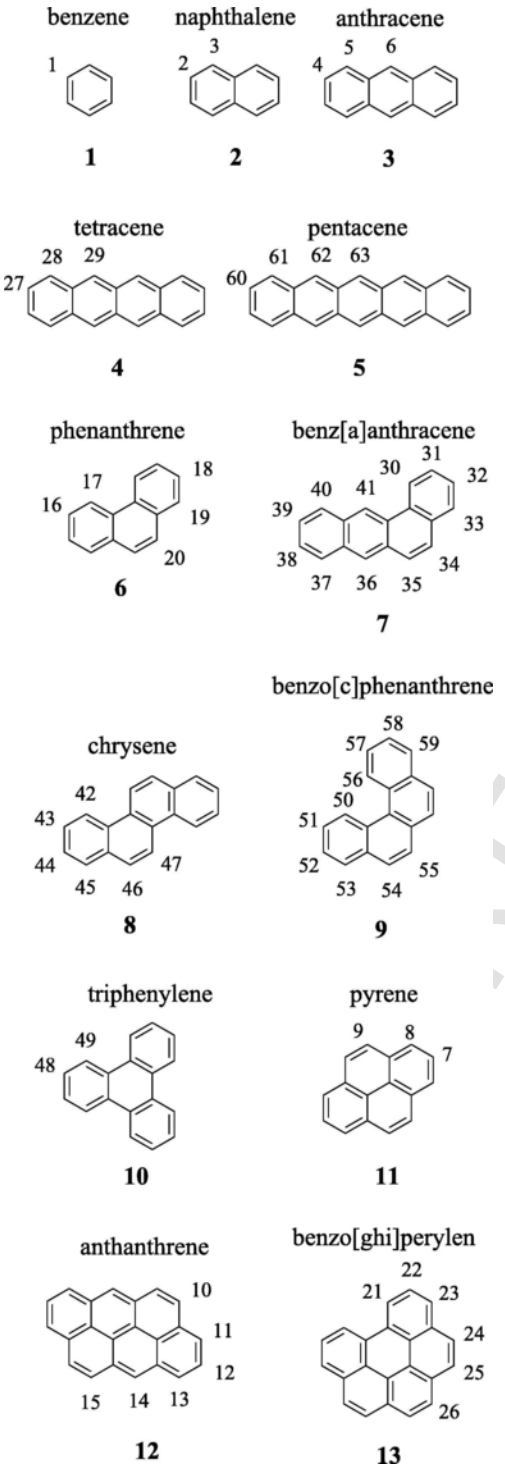


Fig. 2. The set of PAHs. The numbers represent studied reaction sites. Phenanthrene, benz[a]anthracene, chrysene, triphenylene, and benzo[ghi]perylen are the PAHs with bay region(s). Benzo[c]phenanthrene has a fjord region.

2. Computational methods

For the optimizations of initial structures and reaction pathways we used DFT with the meta-GGA functional TPSS [15] and the SVP basis set [16]. The final geometries and electronic energies were obtained with the TPSSh hybrid exchange correlation functional [17] and the TZVP basis set [18] including the D3 dispersion correction [19]. The dispersion correction is included because for large molecules the London interactions have a significant influence on the potential energy surfaces. The zero-point vibrational energy (ZVPE) corrections to the electronic energies were computed at the same electronic structure level (TPSSh-D3/TZVP) within the harmonic approximation. We have used the scaling factor of 0.9874 optimized in Ref. [20] for TPSSh/6-31 + G(d,p) to fit the experimental ZPVE.

All the calculations were performed with the TURBOMOLE program package [21]. For all of the calculations, the resolution of the identity (RI-J) approximation has been used for the Coulomb energy with the optimized auxiliary basis sets from Ref. [22].

The reaction and activation energies are calculated as

$$\Delta E = \sum E^{el}_{products} - \sum E^{el}_{reactants} + \Delta ZPVE, \quad (9)$$

and

$$\Delta E^{\ddagger} = E^{el}_{TS} - \sum E^{el}_{reactants} + \Delta ZPVE. \quad (10)$$

The Gibbs free energies are calculated using the `freeh` program of the TURBOMOLE package. This code calculates the vibrational partition function within the harmonic oscillator approximation and the rotational partition function within the rigid rotor model. Based on the ideal gas assumption for the O and H atoms the internal energy contribution due translations is assumed to be 3R/2, where R is the gas constant, and the PV term of enthalpy is calculated as RT, where P is the pressure, V the molar volume and T the temperature.

3. Accuracy of the results

In order to evaluate the accuracy of the TPSSh-D3/TZVP results, Table 1 compares the reaction energies for benzene **1**, naphthalene **2** for site 2 and 3, and pyrene **11** for site 9 with computational reference data from the literature. The TPSSh-D3/TZVP results are in general less exothermic for the opening of the three-membered rings and the formation of the carbonyl radicals, but the deviations exceed only in two cases ±26 kJ/mol. This is approximately the accuracy obtained at a DFT level for such systems if one takes into account the uncertainties from the transition state optimizations done with different functionals and basis sets.

4. Reaction mechanism and geometrical effects

4.1. Reaction mechanism

The first reaction step that we studied is the addition of $O(^3P)$ to the PAHs which is exothermic. In a subsequent step a hydrogen atom is eliminated and the corresponding oxyradical is formed. Among the PAHs studied (Fig. 2), neither the $O(^3P)$ addition nor the H atom abstraction are geometrically constrained. Therefore, all

Table 1
Comparison of the TPSSh-D3/TZVP energies with the literature. In the nomenclature SX-Y, X = 1,2,3,4,5,6 refers to the reaction step/intermediate with S1: PAH, S2: triplet intermediate after O(^{3}P) addition, S3: oxyradical, S4: radical with cylopropane moeity, S5: carbonyl radical, and S6: final radical with five-membered C-ring. The index Y refers to the reaction site (cmp. Fig. 2).

	$\Delta E^{\ddagger}$ (kJ/mol)		ΔE (kJ/mol)	
	TPSSh-D3	Literature	TPSSh-D3	Literature
S1-1 + O → S2-1	−4.3	17.2[a]	−63.7	−60.7[a]
S2-1 → S3-1 + H	41.1	43.9 [a]	16.9	−5.4[a]
S3-1 → S4-1	199.0	216.3[b]	184.3	192.5[b]
S4-1 → S5-1	29.6	34.7[b]	−35.3	−65.3[b]
S5-1 → S6-1	12.0	23.0[b]	−30.4	−33.5[b]
S3-2 → S4-2	185.9	187.0[c], 197.5[d]	169.9	170.3[c], 183.7[d]
S4-2R → S5-2R	27.9	32.2[c], 29.3[d]	−52.0	−76.6[c], −64.4[d]
S5-2R → S6-2R	13.4	22.2[c], 15.5[d]	−40.9	−50.6[c], −59.4[d]
S4-2L → S5-2L	66.8	82.8[c], 68.2[d]	33.3	10.5[c], 23.8[d]
S5-2L → S6-2L	3.1	18.8[c], 2.1[d]	−126.2	−137.7[c], −147.7[d]
S3-3 → S4-3	241.5	241.8[c], 257.7[d]	239.7	241.4[c], 258.2[d]
S4-3 → S5-3	0.0	2.1[c], 0.4[d]	−105.6	−130.1[c], −120.9[d]
S5-3 → S6-3	13.3	22.2[c], 15.5[d]	−41.0	−50.6[c], −59.0[d]
S3-9 → S5-9	252.7	252.7[e]	146.4	120.9[e]
S5-9 → S6-9	18.4	24.3[e]	−27.5	−42.3[e]

[a] CBS-QB3 energies of the B3LYP/6–311G(d,p) geometry optimized structures from Nguyen et al. [10].
[b] CASPT2/6–31G(d,p) + ZPVE results from Olivella et al. [11].
[c] G3(MP2,CC) energies of the B3LYP/6–311G(d,p) optimized geometries [6].
[d] B3LYP/6–311G(d,p) + ZPVE results from Zhou et al. [6].
[e] G3(MP2,CC) results from Singh et al. [23].

the PAHs studied in this work follow for these steps analogous pathways as benzene (Eq. (2)).

The reaction pathway for CO elimination is well-established for the phenoxy radical (Eq. (9)) but only few and partially contradictory results have been published for larger PAHs. For the solo sites of pentacene it has in Ref. [13], based on the result of a potential energy scan at the B3LYP/6-311(d,p) level, been concluded that reaction pathways similar to that of the phenoxy radical are unlikely. In the current study we were able to find for the solo sites of pentacene the analogous reaction pathway for a single step mechanism. For the solo site 62 of pentacene **5** we obtained the reaction energy as 73.0 kJ/mol and the activation energy as 327 kJ/mol, and for the solo site 63 as 70.9 and 368 kJ/mol, respectively. Both activation energies for the solo sites of pentacene are significantly smaller than the 440 kJ/mol calculated by You et al. [13] for the ring opening at the B3LYP/6-311G(d,p) level.

In another study using B3LYP/6-311 + G(d,p) Liu et al. has found that at the solo site of the benz[a]anthracene (**7**) oxyradical, which is geometrically similar to the solo sites of pentacene, CO eliminates along a similar pathway as for phenoxy radicals with the only difference that the elimination happens in a single step [14]. They reported the activation energies of the CO elimination from the solo (site 36) and bay-solo sites (site 41) of the benz[a]anthracene oxyradical as 348 kJ/mol and 335 kJ/mol respectively [14]. We obtained for the activation energies for these sites at the TPSSh-D3/TZVP level 304 kJ/mol and 312 kJ/mol, respectively. For the bay-solo site (41) the current result is close enough to the value reported by Liu et al. to assume that the two calculations follow a similar reaction parthway; however, for the solo site (36) it deviates significantly. Therefore, we re-optimized for these sites the structures of the oxyradical and transition states (T36) with the B3LYP functional (using the VWN(III) functional) and the 6–311 + G(d,p) basis set. At this level we obtained for the current pathway activation energies of 318 kJ/mol and 332 kJ/mol. At the bay-solo site 41, the geometry of the transition state structure are the same as the one reported by Liu et al.; however, for the solo site 36, as compared with those reported by Liu et al. [14], the transition state structure has the shorter C–C bond length of the cyclopropanone-like moeity at the opposite side and is lower in energy by approximately 30 kJ/mol. A similar difference in the activation energies depending on from which side of the cyclopropanone moeity the CO eliminates can also be seen in Fig. 4. The difference in the activation energies for the S4-12 → S5-12L and S4-12 → S5-12R reactions is 22.5 kJ/mol, which is of the same order of magnitude as the difference between the transition state found for the CO elimination at the solo site 36 in this study and that reported by Liu et al .[14]. That is, the transition states found in this study are comparable to the ones reported in the literature.

Analysis of the reactions at sixty-three sites (Fig. 2) indicates that, in general, the CO elimination from PAH oxyradicals can follow either a three, two, or single step mechanism depending on the geometrical strain at the reaction site. Fig. 3 shows the reaction pathways and Fig. 4 the corresponding intermediates along the reaction pathways for different sites of anthanthrene — an example that illustrate the relation between the site types and the three, two, and single step CO elimination mechanisms. During the O(^{3}P) addition, spin density is transferred from the oxygen atom to the ring system and a C–O σ bond is formed. During the H abstraction, the σ C–H bond of the triplet intermediate structure S2 breaks

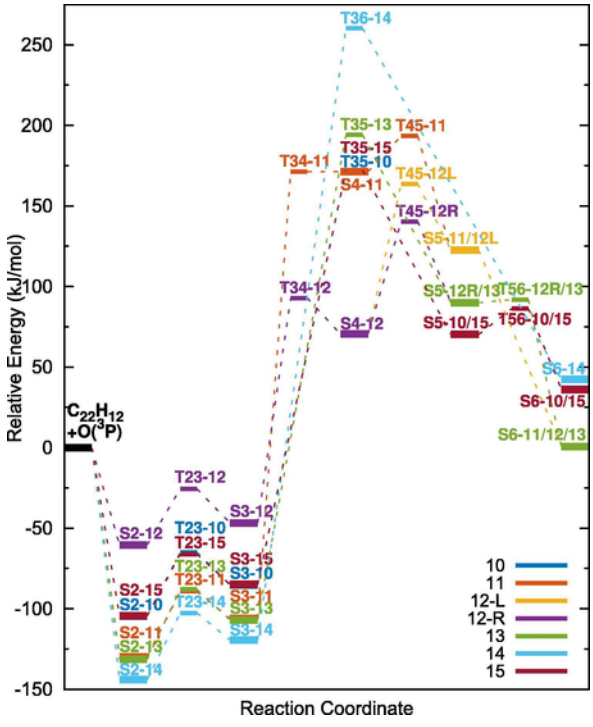


Fig. 3. Reaction profiles for anthanthrene. The corresponding structures are shown in Fig. 4. Site 14 follows a single step CO elimination mechanism, the sites 10, 13, and 15 a two step and sites 11 and 12 a three step CO elimination mechanism.

UNCORRECTED PROOF

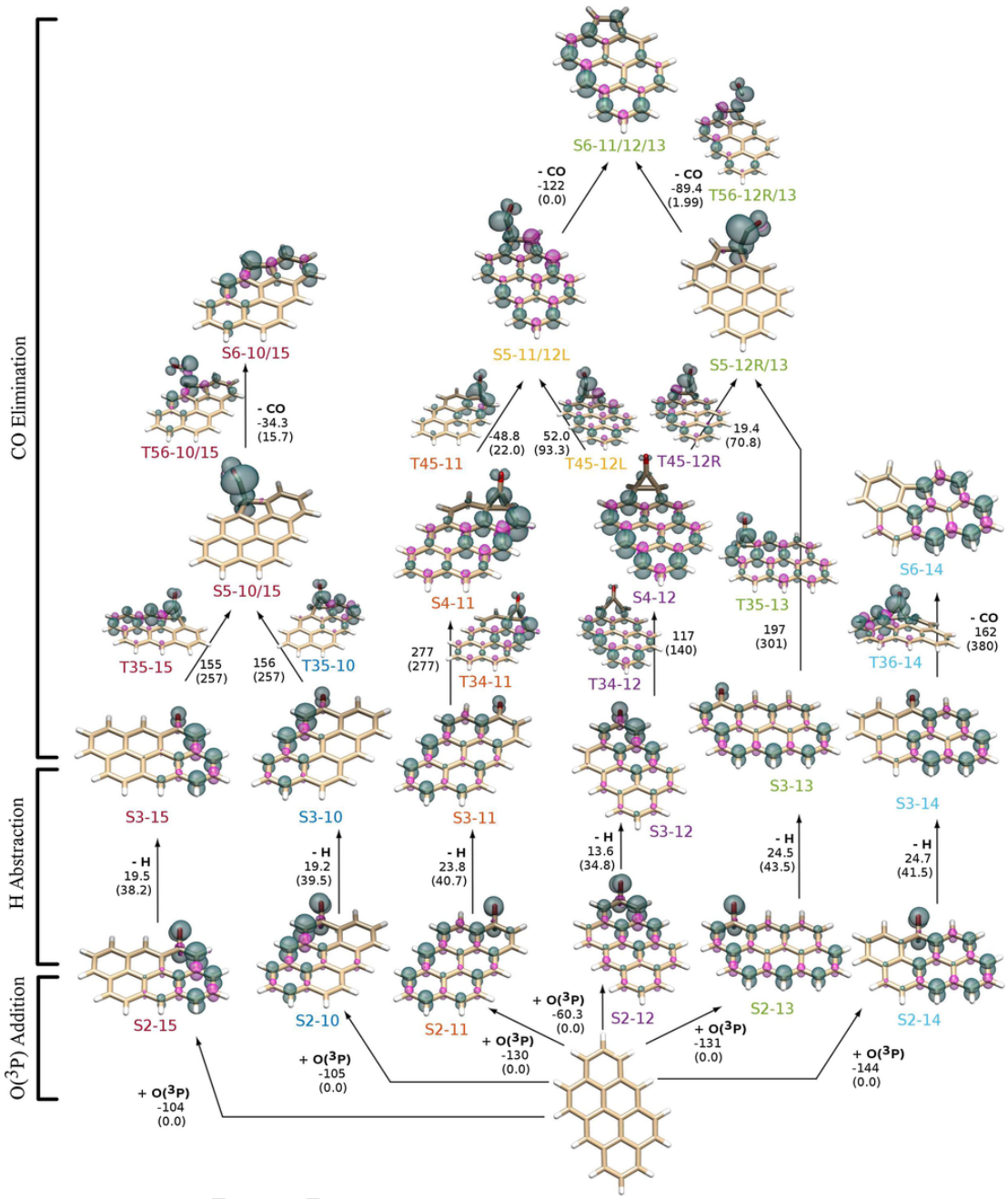


Fig. 4. The intermediates along the reaction pathways of anthanthrene as examples for the three different kinds of pathways. Reacting species are shown with their spin densities. Reaction and activation energies are given in kJ/mol, activation energies are given inside parantheses. The $O(^3P)$ addition step occurs without a barrier for the sites on anthanthrene.

and the oxygen forms a π bond which is conjugated with the π system of the aromatic carbon rings. The doublet oxyradical can then undergo the CO elimination reaction. As can be seen from these figures, the three step CO elimination mechanism is analogous to that of the phenoxy radical sketched in Eq. (8). For this mechanism the second step, which is the ring opening of the cyclopropanone moeity to a carbonyl radical, possess the overall highest barrier along the reaction pathway. Therefore, this step is the rate limiting step for the three step CO elimination mechanism. For the two step mechanism the structures with a strained three-membered carbon ring, which are the intermediates formed in the first step of the three step mechanism (S4 structure) are not local minima along the reaction pathway. However, the transition state of the first step of the two step mechanism (T35 structures) have a similar structure with a three-membered carbon as the intermediates S4 of the three step mechanism. The CO elimination from carbonyl radicals for the two and three step mechanisms are analogous and comparable. In the single step mechanism none of the two intermediates (S4 and S5 structures) are formed. But again, the transition state structure T36-14 is similar to the S4 structure of the three-step mechanism.

4.2. First step of CO elimination and geometrical effects

The geometrical strain can be related to the site type (quartet, trio, duo, or solo) and the number of neighboring rings. Among the sample set of PAHs, the quartet sites exist in the acenes (**2**–**5**) and

phenacenes (**6**, **8**) as well as in benz[a]anthracene (**7**), benzo[c]phenanthrene (**9**), and triphenylene (**10**). Trio sites are found in the peri-fused PAHs (**11**–**13**), and duo sites in the phenacenes (**6**,**9**), benz[a]anthracene (**7**), benzo[c]phenanthrene (**9**), and peri-fused PAHs (**11**–**13**). Solo sites occur in our sample set in the acenes larger than naphthalene (**3**–**5**) and anthanthrene (**12**). The quartet and trio sites have in addition different reactivities when they are located at an inner (α carbon) or outer (β carbon) positions (see Fig. 2), – the former are geometrically more constrained and require higher activation energies for reactions that involve a ring deformation.

Table 2 shows the ranges of activation energies of the first step of the CO elimination sorted according to the site type and the number of neighboring rings. For the three step CO elimination mechanism from the oxyradicals, this corresponds to the isomerization of the oxy- to cyclopropanone radicals. Among the reaction sites in the test set which follow the three step CO elimination mechanism, the most reactive ones are the outer trio sites with activation energies ranging from 140 to 162 kJ/mol. They are followed by the outer quartet sites with activation energies ranging from 170 to 194 kJ/mol. The activation energies of the inner quartet sites ($189<\Delta E^{\ddagger}$ (kJ/mol)<242) are higher than for the outer quartet sites. The activation energies for duo sites with two neighboring rings ($182<\Delta E^{\ddagger}$ (kJ/mol)<220) are in between those of two types of quartet sites.

Table 2
Activation energies of the first step of CO elimination ($\Delta E^{\ddagger} = E_{T3X} - E_{S3} + \Delta ZPVE$ where X = 4,5,6 for three, two, and single step mechanisms respectively) in kJ/mol. The range of activation energy for each site type indicates that geometrical strain at the reaction site determines the CO elimination mechanism and activation energy.

CO abstraction mechanism	Site type		$\Delta E^{\ddagger}$ range (kJ/mol)
Three step	Outer trio		140–162
	Outer quartet		170–194
	Duo & 2 neighbors		184–220
	Inner quartet		189–242
	Inner trio (except anthanthrene)		236–277
Two step	Duo & 3 neighbors		240–257
	Inner trio @anthanthrene		301
Single step	Solo & 2 neighbors		304–368
	Solo & 4 neighbors (@anthanthrene)		380

The sites follow the two or the single step CO elimination mechanism when the geometrical strain raises the energy for the cyclopropanone structure so much that it becomes instead of an intermediate a transition state. For the duo sites with three neighboring rings, CO elimination occurs in two steps. The range of activation energies for the first reaction step is for these sites with 240–257 kJ/mol similar to that for the inner trio sites which follow the three step mechanism. On the other hand, the inner trio sites still follow a three step mechanism with the exception of site 13 in anthanthrene **12**. The activation energies of the trio sites are in the range 236–277 kJ/mol, which is higher than that for the duo sites with three neighboring rings although the trio sites are geometrically less constraint. Among the inner trio sites, site 21 at the bay region of benzo[ghi]perylen **13** has the lowest activation energy due to its flexibility. In contrast to this, the exceptional inner trio site 13 of anthanthrene **12** has a very high activation energy of 301 kJ/mol. The reaction at this site occurs in a two step mechanism. In general, the activation energies for the CO elimination are for the solo sites the highest among all the sites studied in this work. The highest activation energy of 380 kJ/mol belongs to the solo site 14 in anthanthrene **12** which has four neighboring rings.

This analysis of the activation energies for the first step of the CO elimination for different types of sites indicates that as the geometric constrains at the reaction site increases also the activation energy of this step increases. However, we could not find a quantitative measure for only the geometrical strain without including electronic effects from the aromatic π system, and therefore we could not also find a quantitative relation of it to the activation energy of the first step of the CO elimination from oxyradicals.

5. Electronic effects

5.1. Hückel molecular orbital theory analysis

The O(^{3}P) addition to PAHs, the subsequent H abstraction which leads to the oxyradicals, and the CO elimination from carbonyl radicals are expected to be dominated by electronic effects from the π-system. To better understand the differences and trends in the reaction energies for these steps we made an analysis based on the Hückel molecular orbital theory (HMOT). In HMOT only the π-electrons are considered and thus the energies obtained from it can be used as a measure of the resonance energy, i.e. the electronic stabilization due to delocalization of the electrons in the aromatic ring system. To evaluate the effect of rearrangements in the π-electron system on the variation of the reaction energies, we have calculated resonance energies for π system analogues of the actual reaction intermediates shown in Table 3. These were chosen such that they have the same atoms and the same number of electrons in the π-system as the actual reaction intermediates but are planar and describable by HMOT. The contribution of the π-system to the reaction energy has been calculated for each reaction and site by taking the difference in the total resonance energies of the analogues for the reactant and the product.

Fig. 5 shows correlation plots where the reaction energies for the O(^{3}P) addition, the H abstraction, and the CO elimination from carbonyl radicals are compared with the contribution from the resonance energy obtained from HMOT. According to this analysis, the correlation between the actual reaction energies and the contribution from change in resonance energy is only weak for the H abstraction, but for the O addition and CO elimination there is a strong

UNCORRECTED PROOF

Table 3
The σ-framework of the structures used for the reaction of benzene in the HMOT analysis. The PAH analogues are used for the HMOT analysis of the influence of the π-electron delocalization on the reaction energies.

	Reactant	Product
$O(^3P)$ Addition		
H Abstraction		
CO Elimination		

correlation. These results indicate that the contribution from the π-orbital rearrangements to the reaction energies play a major role for the O addition and CO elimination; on the other hand, for the H abstraction other effects are equally important.

5.2. Site specific analysis: $O(^3P)$ addition

The strong correlation between the changes in the resonance energy and the reaction energies for the $O(^3P)$ addition to PAHs, indicates that mainly electronic effects from the aromatic π-system are responsible for differences in the reactivity of different sites. In order to further analyze the relation between the reaction energies and particular site types and the size of the PAHs, Fig. 6 shows the reaction energies at each studied reaction site.

For the linear PAHs **2**–**5** the reaction becomes in general more exothermic with increasing size of the PAH. Similarly, when we compare the sites of pyrene **11** (−50.8, −110, −98.0 kJ/mol) with analogous trio and duo sites of anthanthrene **12** (−60.3, −130/−131, −105/−104 kJ/mol), the energy release is higher for the larger PAH anthanthrene **12**. The increasing exothermicity of the $O(^3P)$ addition to PAHs with increasing size of the aromatic system can be explained by the increasing delocalization of the unpaired electron in the product.

Another observation is that for the linear molecules (**2**–**5**) the reaction at the inner quartet site is more exothermic than at the outer quartet site, and that the solo sites on the inner ring are for this elementary step the most reactive sites. There are similarities between these patterns and the reactivity patterns described for the Diels–Alders reactions. For this class of reactions it has also been found that the reactivity of acenes increases with increasing size of the PAH and that the central ring is the most reactive one [24].

Lastly, when the PAH is branched the $O(^3P)$ addition becomes in many cases less exothermic, e.g. when we compare analogous sites in anthracene **3** (−93.2, −108 kJ/mol) and phenanthrene **6** (−74.8/−69.3, −86.4/−88.6 kJ/mol) or in anthanthrene **12** (−105/−104, −130/−131, −60.3 kJ/mol) and benzo[ghi]perylen **13** (−102/−96.4/−102, −109/−107, −58.5 kJ/mol).

5.3. Site specific analysis: The CO elimination from carbonyl radicals

The reaction energies of the CO elimination from carbonyl radicals at different sites are shown in Fig. 7. For the linear acenes this elementary step does not occur at the outer site of five membered rings when the initial PAH is larger than anthracene even though before the isomerization the site was a quartet site. The reason is the lower stability of the intermediate carbonyl radical at the outer quartet site compared to the inner quartet site. This stability difference increases with the length of the acenes, which is an electronic effect from the π-sytem: For naphthalene **2**, anthracene **3**, tetracene **4**, and pentacene **5** the difference in the resonance energies between the carbonyl radicals at inner and outer sites of the five membered ring obtained from HMOT are respectively 0.4, 0.6, 0.6, and 0.7 β. As a consequence of this, only the more stable carbonyl radicals at the inner sites are formed in the preceding step of the CO elimination.

Additionally, for the CO abstraction from the carbonyl radicals we find the trend that the reaction becomes for analogous sites more exothermic with increasing size of the PAHs. Finally, if the pathway exists, the CO at the outer position abstracts significantly more exothermic than the one at the inner position, which is again a consequence of the different stabilities of the two isomeric structures for the carbonyl radicals.

6. Relation of the reaction and activation energies

Since the localization of reaction pathways and transition states is computationally much more demanding than the optimization of

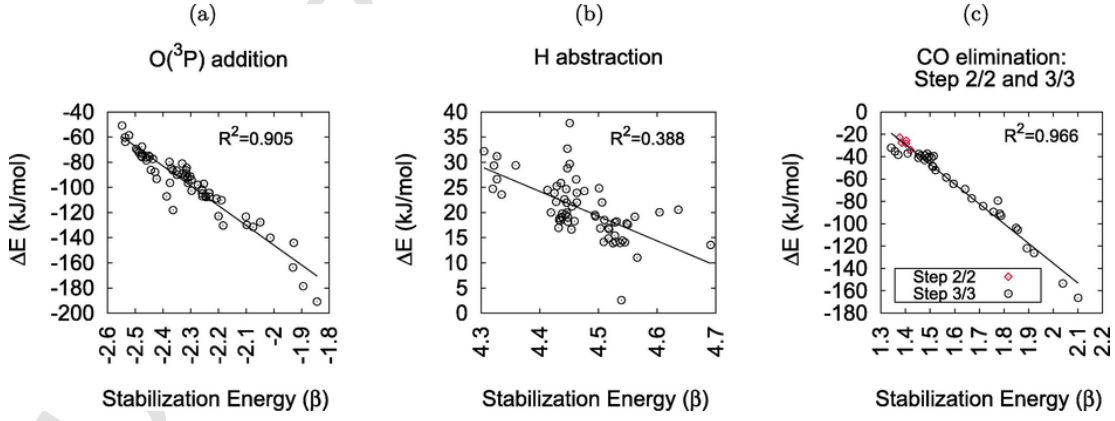


Fig. 5. Reaction energies calculated by DFT plotted versus the change in the resonance energies obtained from HMOT for (a) the $O(^3P)$ addition to PAHs ($\Delta E/kJ\cdot mol^{-1} = -157\ E_{stabilization}/\beta - 461$, s = 8 kJ·mol^{-1}, R^2 = 0.905), (b) the subsequent H abstraction to from the oxyradical ($\Delta E/kJ\cdot mol^{-1} = -49.2\ E_{stabilization}/\beta + 241$, s = 5 kJ·mol^{-1}, R^2 = 0.388), and (c) CO elimination from carbonyl radicals ($\Delta E/kJ\cdot mol^{-1} = -177\ E_{stabilization}/\beta + 219$, s = 7 kJ·mol^{-1}, R^2 = 0.966). Benzene is excluded. β is negative as it represents the (stabilizing) resonance energy for an isolated π bond. R^2 is the coefficient of determination and s the standard deviation of the fit.

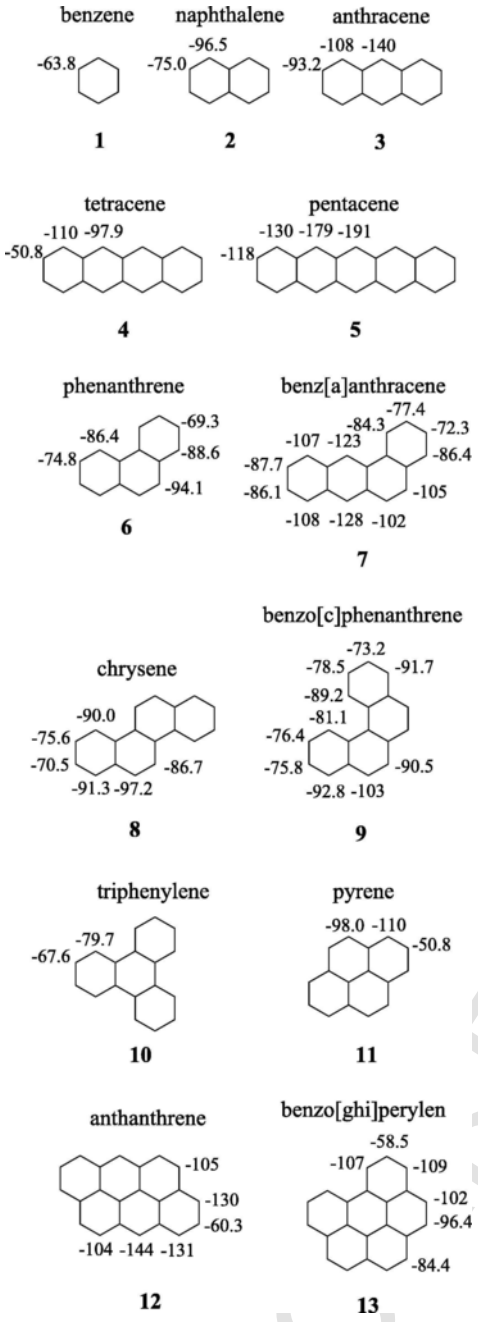


Fig. 6. Reaction energies for the O(^{3}P) addition to PAHs for each studied site in kJ/mol. For clarity only the σ-bond network of the carbons is shown.

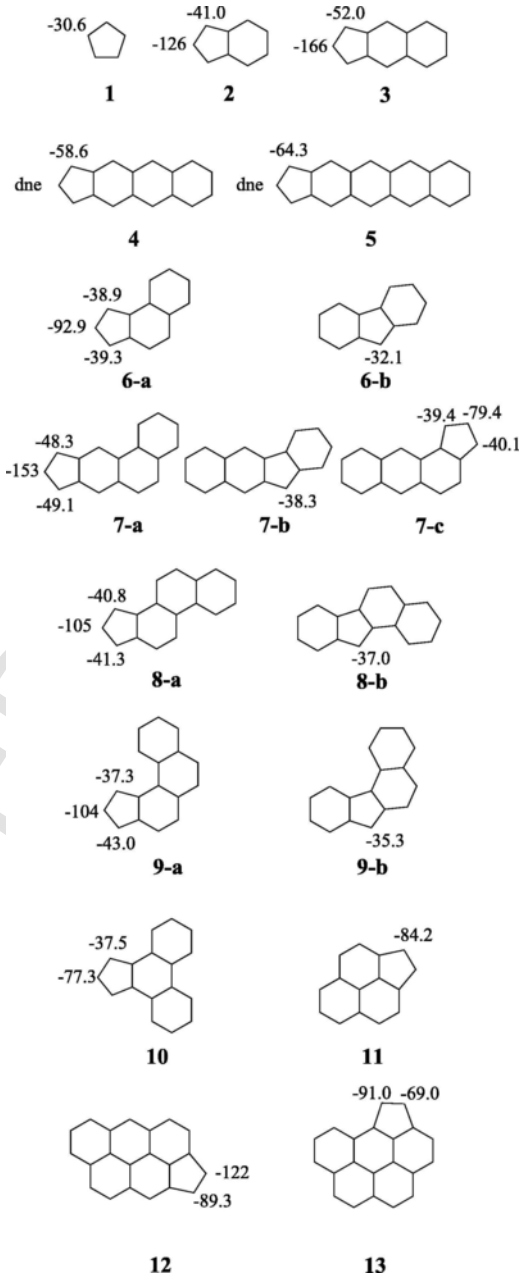


Fig. 7. Reaction energies of the CO elimination from carbonyl radicals in kJ/mol. Only the σ-bonding network of carbons are shown for the final polyaromatic structures. Some of the shown structures (**7-b**, **8-b**, **9-b**) and some other polyaromatics with a five-membered ring polyaromatics may be formed through single step CO elimination mechanism. However; as in such a case the reaction energy is dependent on the geometrical strain and CO eliminates in a single step, they are irrelevant in this discussion.

the structures of the reactants and products, it is desirable to find a correlation between reaction and activation energies that can be used to extrapolate the results from the sample set to other molecules. Therefore, we analyzed the degree of correlation for each reaction step by means of Bell-Evans Polanyi (BEP) [25,26] plots which are shown in Fig. 8. For all reaction steps there is at least a general trend of a BEP correlation. However, we also note that some mechanism are sampled by our test set more than the others. For example, the set of sites corresponding to PAHs consists of thirty-four quartet, thirteen duo, eight trio, and seven solo sites; or among the sixty-three sites there are only seven sites at bay regions and only one site at a fjord region.

For the O(^{3}P) addition, the more exothermic the reaction is, the lower is the activation energy $\Delta E^{\ddagger}$. The negative activation energies are due to the way reaction and activation energies are calculated according to Eq. (10) relative to the fully separated, i.e. isolated, reactants. When calculated with respect to the shallow van der Waals (vdW) minima, the activation energies are positive. For example, if it is calculated from Eq. (10), for site number 1 at benzene (**1**) $\Delta E^{\ddagger}$ is −4.34 kJ/mol. On the other hand, when calculated with respect to the intermediate vdW minimum of the reactants, it is 7.51 kJ/mol. Similarly, the activation energies $\Delta E^{\ddagger}$ calculated according to Eq. (10) relative to the isolated reactants and relative to

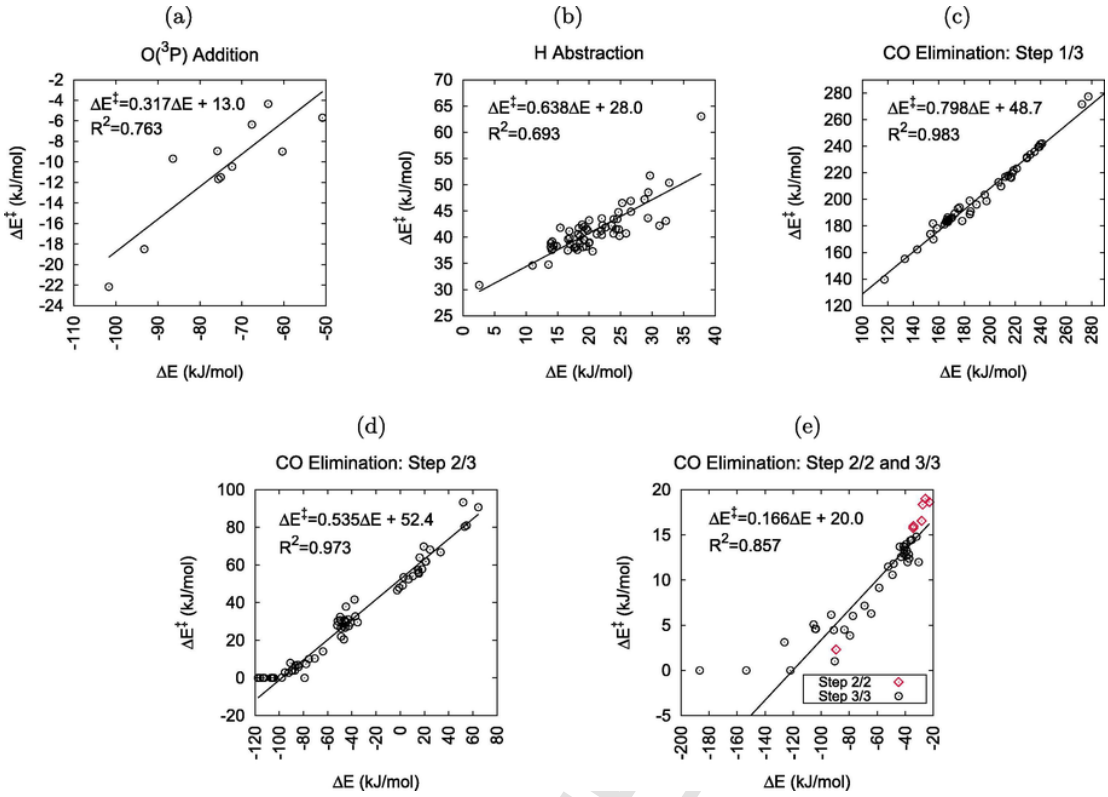


Fig. 8. BEP plots. (a) O(^{3}P) addition to PAHs, s = 2.7 kJ/mol, (b) following H abstraction to form oxyradical. (s = 2.5 kJ/mol) (c) First step of the three step CO elimination mechanism from the oxyradicals, s = 3.8 kJ/mol. (d) Second step of the three step CO elimination mechanism, s = 4.1 kJ/mol. (The points for which the activation energy is zero are excluded in the fit.) (e) CO elimination from carbonyl radicals, s = 1.9 kJ/mol. (The points for which the activation energy is zero are excluded in the fit.) The constant terms in the correlation equations has kJ/mol as units.

the vdW minima are, respectively, −11.5 and 7.39 kJ/mol for site 2, −10.5 and 8.02 kJ/mol for site 32, −22.2 and 1.93 kJ/mol for site 35, and, finally, −11.7 and 6.8 kJ/mol for site 43. The BEP plot of the O(^{3}P) addition has a slope less than 0.5 indicating a reactant-like early transition state. As the reaction gets exothermic, the activation energy becomes zero. Additionally, the more exothermic the reaction, the earlier is the transition state as evidenced by the larger C–O distance, in accordance with Hammond's postulate [27] as can be seen from Fig. 9a.

The H abstraction has a transition state structure similar to the products, which results in a BEP fit with a slope larger than 0.5 (Fig. 8b). The outlier at $\Delta E^{\ddagger}$ = 63.0 kJ/mol and ΔE = 37.8 kJ/mol correspond to the site 56 of benzo[c]phenanthrene **9** which is a site at the fjord region. The reason that the activation energy is in this case higher than the BEP fit is probably that the repulsive close H···H and the attractive H···O contacts in the fjord region lead to an additional stabilization of the non-planar structure of intermediate S2–56 relative to the more planar structure of the oxyradical as illustrated in Fig. 10. Similar as for the O(^{3}P) addition and in accordance with Hammond's postulate, the more endothermic the H abstraction is, the later the transition state and the larger is the C–H distance in the transition state, as can be seen from Fig. 9b.

Finally, we see from the BEP plot for the CO elimination in Fig. 8c that the first step of the three step mechanism shows a very good correlation. Also the second step of the three step CO elimination mechanism shows a very good BEP correlation (see Fig. 8d).

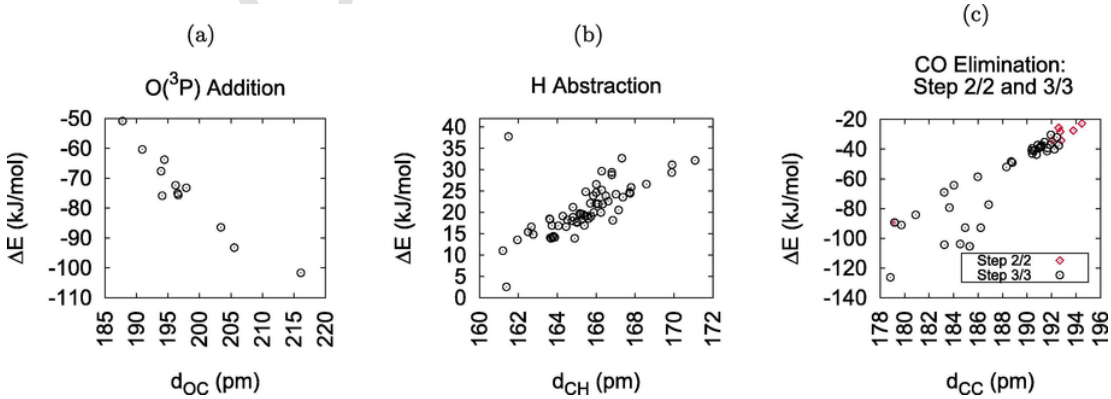


Fig. 9. Hammond postulate. (a) Reaction energy for the O(^{3}P) addition plotted versus the C–O bond length at the transition state. (b) Reaction energy for the H abstraction plotted versus the C–H bond length of the transition state structure. (c) Reaction energy for the CO elimination from carbonyl radicals plotted versus the bond length of the C–C bond that is broken for the transition state structure.

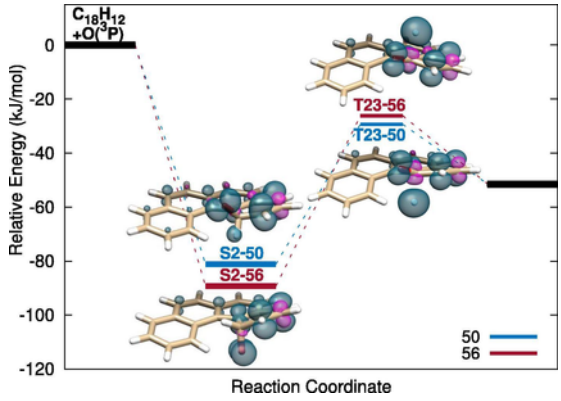


Fig. 10. Reaction path of oxyradical formation on the sites 50 and 56 at the fjord region of benzo[c]phenanthrene. The structures are shown with their spin densities.

The BEP correlation for last step of the two and the three step CO elimination mechanisms resemble each other. Therefore, they are plotted at the same BEP plot in Fig. 8e. Fig. 9c shows the C–C(O) distance of the transition state structure for this reaction step. We observe again in accordance with Hammond's postulate the general trend that the less exothermic the reaction, the later the transition state which in case means a larger the C–C(O) distance. As the sample of PAHs studied in this work contains only few sites where the CO elimination follows the two or the single step mechanism, we refrained from analyzing them further. Since for them the activation barriers for the CO elimination are considerably higher than for the sites where the elimination follows the three step mechanism, they are not expected to contribute significantly to the overall reaction rates for PAH oxidation.

The above analysis was done based on the reaction energies. Fig. S1 in the Supplementary Information shows BEP plots based on the Gibbs free energies for three of the reaction steps calculated using the vibrational, rotational, and translational contributions to the enthalpy and the entropy at 1200 K and 0.1 MPa. For the H abstraction and the CO elimination from carbonyl radicals, the BEP correlation based on Gibbs free energies is weak and there is only a general trend. Nonetheless, for the first and second step of the three step CO elimination mechanism, which are the rate determining steps, the BEP plots based on the Gibbs free energies still show a good correlation.

7. Summary and conclusions

For a qualitative analysis we have studied the reaction and activation energies of the reactions of PAHs with O(^{3}P) using the TPSSh density functional, Grimme's D3-dispersion correction, and the TZVP basis set based on a test set which samples different molecular regions and sizes of PAHs. Specifically we have studied i) the O(^{3}P) addition, ii) the subsequent H abstraction leading to an oxyradical intermediate, and iii) the CO elimination from the oxyradicals. We found that depending on the geometrical strain at the reaction site, the CO elimination takes place in either three steps, two steps, or a single step. Based on a HMOT analysis we could document that the changes in the resonance energy of the aromatic π system are responsible for the different reactivities of the different reaction sites for the O(^{3}P) addition and the release of CO from carbonyl radicals.

The BEP correlation found for all the reactions studied in this work allows us to extrapolate the activation energies for other PAHs based on the reaction energies within $\approx \pm$ 4 kJ/mol for the rate limiting step of the three step CO elimination mechanism. This will facilitate the prediction of the activation energies for the studied reactions for larger systems, and most likely such BEP correlations can be transferred to other reactions that occur during the combustion of PAHs and the char burnout.

8. Associated content

The Supplementary Information includes tables of electronic energies calculated at TPSSh-D3/TZVP level, the zero point energy corrections, the contributions of vibrational, rotational, and translational partition functions to entropy and enthalpy at 1200 k and 0.1 MPa. Additionally, the BEP plots based on Gibbs free energy differences for some of the reaction steps are given.

Acknowledgment

This work was financially supported by the German Research Foundation (DFG) within the framework of the SFB/Transregio 129 Oxyflame.

Appendix A. Supplementary data

Supplementary data associated with this article can be found, in the online version, athttps://doi.org/10.1016/j.fuel.2018.12.047.

References

[1] B. Buhre, L. Elliott, C. Sheng, R. Gupta, T. Wall, Oxy-fuel combustion technology for coal-fired power generation, Prog Energy Combust Sci 31 (2005) 283–307, https://doi.org/10.1016/j.pecs.2005.07.001.
[2] M. Keiluweit, P.S. Nico, M.G. Johnson, M. Kleber, Dynamic molecular structure of plant biomass-derived black carbon (biochar), Environ Sci Technol 44 (4) (2010) 1247–1253, pMID: 20099810. doi: https://doi.org/10.1021/es9031419.
[3] The combustion rates of coal chars: A review, Symposium (International) on Combustion 1982;19(1):1045–65, nineteenth Symposium (International) on Combustion. doi: https://doi.org/10.1016/S0082-0784(82)80281-6.
[4] Char structural ordering during pyrolysis and combustion and its influence on char reactivity, Fuel 2002;81(9):1215–25. doi: https://doi.org/10.1016/S0016-2361(02)00035-2.
[5] R. Harvey, Polycyclic aromatic hydrocarbons: chemistry and carcinogenicity, cambridge monographs on cancer research, Cambridge University Press, 1991.
[6] C.-W. Zhou, V.V. Kislov, A.M. Mebel, Reaction mechanism of naphthyl radicals with molecular oxygen. 1. Theoretical study of the potential energy surface, J Phys Chem A 116 (6) (2012) 1571–1585, pMID: 22239650. doi: https://doi.org/10.1021/jp2119313.
[7] J.L. Emdee, K. Brezinsky, I. Glassman, A kinetic model for the oxidation of toluene near 1200 K, J Phys Chem 96 (5) (1992) 2151–2161, https://doi.org/10.1021/j100184a025.
[8] K. Brezinsky, The high-temperature oxidation of aromatic hydrocarbons, Prog Energy Combust Sci 12 (1) (1986) 1–24.
[9] C.A. Taatjes, D.L. Osborn, T.M. Selby, G. Meloni, A.J. Trevitt, E. Epifanovsky, et al., Products of the benzene + O(^{3}P) reaction, J Phys Chem A 114 (9) (2010) 3355–3370, pMID: 20099861. doi: https://doi.org/10.1021/jp9114145.
[10] T.L. Nguyen, J. Peeters, L. Vereecken, Theoretical reinvestigation of the O(^{3}P) + C_6H_6 reaction: quantum chemical and statistical rate calculations, J Phys Chem A 111 (19) (2007) 3836–3849, pMID: 17253662. doi: https://doi.org/10.1021/jp0660886.
[11] S. Olivella, A. Sole, A. Garcia-Raso, Ab initio calculations of the potential surface for the thermal decomposition of the phenoxyl radical, J Phys Chem 99 (26) (1995) 10549–10556, https://doi.org/10.1021/j100026a018.
[12] R. Liu, K. Morokuma, A.M. Mebel, M.C. Lin, Ab initio study of the mechanism for the thermal decomposition of the phenoxy radical, J Phys Chem 100 (22) (1996) 9314–9322, https://doi.org/10.1021/jp953566w.
[13] X. You, D.Y. Zubarev, W.A. Lester, M. Frenklach, Thermal decomposition of pentacene oxyradicals, J Phys Chem A 115 (49) (2011) 14184–14190, pMID: 22054037. doi: https://doi.org/10.1021/jp208974b.
[14] P. Liu, H. Lin, Y. Yang, C. Shao, C. Gu, Z. Huang, New insights into thermal decomposition of polycyclic aromatic hydrocarbon

UNCORRECTED PROOF

oxyradicals, J Phys Chem A 118 (48) (2014) 11337–11345, pMID: 25386793. doi: https://doi.org/10.1021/jp510498j.
[15] J. Tao, J.P. Perdew, V.N. Staroverov, G.E. Scuseria, Climbing the density functional ladder: nonempirical meta generalized gradient approximation designed for molecules and solids, Phys Rev Lett 91 (2003)146401https://doi.org/10.1103/PhysRevLett. 91.146401.
[16] A. Schäfer, H. Horn, R. Ahlrichs, Fully optimized contracted Gaussian basis sets for atoms Li to Kr, J Chem Phys 97 (4) (1992) 2571–2577.
[17] V.N. Staroverov, G.E. Scuseria, J. Tao, J.P. Perdew, Comparative assessment of a new nonempirical density functional: Molecules and hydrogen-bonded complexes, J Chem Phys 119 (23) (2003) 12129–12137, https://doi.org/10.1063/1.1626543.
[18] A. Schäfer, C. Huber, R. Ahlrichs, Fully optimized contracted Gaussian basis sets of triple zeta valence quality for atoms Li to Kr, J Chem Phys 100 (8) (1994) 5829–5835.
[19] S. Grimme, J. Antony, S. Ehrlich, H. Krieg, A consistent and accurate ab initio parametrization of density functional dispersion correction (DFT-D) for the 94 elements H-Pu, J Chem Phys 132 (15) (2010)154104https://doi.org/10.1063/1.3382344.
[20] G.I. Csonka, A. Ruzsinszky, J.P. Perdew, Estimation, computation, and experimental correction of molecular zero-point vibrational energies, J Phys Chem A 109 (30) (2005) 6779–6789, pMID: 16834032. doi: https://doi.org/10.1021/jp0519464.
[21] TURBOMOLE V7.1 2016 and V7.2 2017, a development of University of Karlsruhe and Forschungszentrum Karlsruhe GmbH, 1989–2007, TURBOMOLE GmbH, since 2007; available from http://www.turbomole.com.
[22] K. Eichkorn, F. Weigend, O. Treutler, R. Ahlrichs, Auxiliary basis sets for main row atoms and transition metals and their use to approximate Coulomb potentials, Theoret Chem Acc 97 (1) (1997) 119–124, https://doi.org/10.1007/s002140050244.
[23] R.I. Singh, A.M. Mebel, M. Frenklach, Oxidation of graphene-edge six- and five-member rings by molecular oxygen, J Phys Chem A 119 (28) (2015) 7528–7547, pMID: 25894330. doi: https://doi.org/10.1021/acs.jpca.5b00868.
[24] P.V.R. Schleyer, M. Manoharan, H. Jiao, F. Stahl, The acenes: is there a relationship between aromatic stabilization and reactivity?, Organic Lett 3 (23) (2001) 3643–3646, pMID: 11700102. doi: https://doi.org/10.1021/ol016553b.
[25] The theory of reactions involving proton transfers, Proceedings of the Royal Society of London A: Mathematical, Physical and Engineering Sciences 154 (882) (1936) 414–429. doi: https://doi.org/10.1098/rspa.1936.0060.
[26] M.G. Evans, M. Polanyi, Inertia and driving force of chemical reactions, Trans Faraday Soc 34 (1938) 11–24, https://doi.org/10.1039/TF9383400011.
[27] G.S. Hammond, A correlation of reaction rates, J Am Chem Soc 77 (2) (1955) 334–338, https://doi.org/10.1021/ja01607a027.

UNCORRECTED PROOF